Characterization of a Visible-Light Spectrometer in the Littrow Configuration

Neil Ghugare

The Ohio State University, Department of Physics, Columbus, OH 43210

April 30, 2026

Abstract

This experiment describes the characterization and calibration of a grating spectrometer used in the Littrow configuration to perform high-resolution visible spectroscopy. We initially calibrated using a monochromatic laser ($\lambda_{\text{laser}} = 517$ nm) and then used a Helium gas tube to determine the grating constant d, found to be 834.4 ± 1.3 nm. We analyzed the spectrometers resolving power using a sodium gas lamp, and then verified the calibrated model by analyzing emission spectra of known gases: Xenon, Mercury, and Hydrogen. We performed a secondary calibration using Argon fringes to establish a pixel-to-wavelength conversion factor. We used these combined calibration techniques on an unknown gas sample, determined to be Krypton gas based on a reduced $\chi^2 = 0.54$. Finally, we briefly discuss the implications of these results in the context of modern astronomy and determination of chemical composition of distant stellar and galactic bodies.

1 Introduction

Spectroscopy serves as a foundational pillar of modern physics, providing the experimental evidence necessary for the development of quantum mechanics and the Bohr model of the atom [1]. By analyzing the discrete emission lines of atomic gases, researchers can probe the quantized energy levels of electronic transitions, a technique that remains essential in fields ranging from astrophysics to materials science [1]. In this experiment, we constructed and characterized a visible-light spectrometer to demonstrate the utility of grating-based spectral analysis.

The experimental setup utilizes a reflection grating in the Littrow configuration [2]. This specific geometry, where the incident light and the diffracted light follow the same path, simplifies the grating equation and maximizes the efficiency of the instrument for specific wavelengths [2]. We characterized the spectrometer's performance by measuring the angular displacement of a known laser source and calculating the grating's groove density.

Here we show the successful characterization of the spectrometer, finding a grating constant of $d = 834.4 \pm 1.3$ nm. Using this calibrated instrument, we analyzed the emission spectrum of known gases and an unknown gas. By comparing the measured wavelengths to NIST Atomic

Spectra Database, we identified the unknown sample as Krypton gas. We then briefly discuss the importance of these results to modern astronomy of celestial bodies.

2 Theory

The operation of a grating spectrometer is governed by the principle of multi-slit interference [2]. When light of wavelength λ is incident on a diffraction grating with a groove spacing d at an angle α, the light is diffracted into discrete integer orders m at angles β according to the grating equation [2]:

$$m\lambda = d\left(\sin(\alpha) + \sin(\beta)\right), \tag{1}$$

derived in Supplement A.

This experiment uses the Littrow configuration, a specific geometry where the grating is tilted such that the diffracted light returns along the same path as the incident light ($\alpha = \beta$) [2]. Under this condition, Eq. 1 simplifies to:

$$m\lambda = 2d\sin(\alpha). \tag{2}$$

This configuration is advantageous because it maximizes the grating's efficiency and simplifies the alignment of the optical system [2]. By measuring the angular displacement required to reflect a known laser wavelength (λ_{laser}) back into the source, the grating constant $1/d$ (lines/mm) can be determined [2].

Atomic emission spectra arise from transitions between discrete, quantized energy levels within an atom [1]. When we excite a gas sample (e.g., Helium) via electrical discharge, electrons are promoted to higher energy states [1]. As these electrons decay to lower potential states, they emit photons with energies strictly defined by the difference between two states ΔE [1]. The relationship between this energy change and the observed wavelength λ is governed by the Planck relation $\Delta E = hc/\lambda$ [1]. Because each element possesses a unique configuration, the resulting energy level structure produces a distinct set of emitted wavelengths that serves as a chemical "fingerprint" [1]. The spectrometer functions by spatially resolving these discrete wavelengths, allowing us to identify atomic species by comparing experimental peaks to known transition data [2].

3 Experimental Methods

3.1 Spectrometer Construction and Laser Calibration

We assembled the spectrometer on a rotational stage using a reflection grating with a nominal groove density of 1200 lines/mm [2]. To characterize the instrument, we used a laser ($\lambda_{\text{laser}} =$ 517 nm) as a calibration source [2]. We positioned the grating such that the incident beam was normal to the grating surface [2]. We then rotated the stage to achieve the Littrow configuration, where the first-order diffraction beam was reflected back into the slit. We aligned the zero-order

reflection with the angular stage with a reading of 0° 0'. The angular difference between the $m = \pm 1$ orders allowed us to calculate d from Eq. 2. The laser setup is shown in Fig. 1.

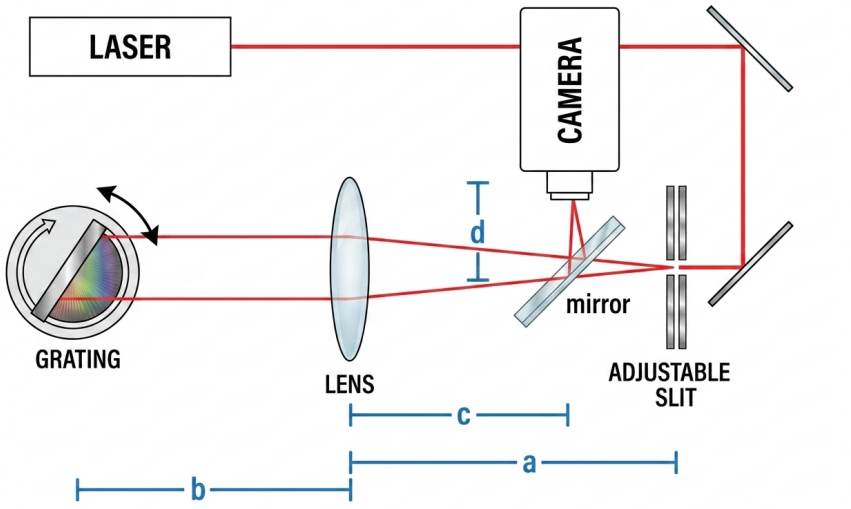

Figure 1: Diagram of our apparatus. Light (either laser light or a gas discharge tube) travels through the adjustable slit, is collimated by the lens, and lands on the grating [2]. The light is reflected by the grating, such that the Littrow configuration is satisfied, and back through the lens to a semi-circular mirror, which focuses the light on a CCD camera for capturing [2]. It is important to keep focal distances accurate, with $a = b = c + d$ and these must equal the focal length of the lens itself [2].

3.2 Resolution and Analysis of Known Gases

After calibration, we replaced the laser with various gas discharge tubes positioned behind a narrow entrance slit, with the diffracted light focusing on a CCD camera [2]. We used a sodium gas tube to analyze the resolving power $\mathscr{R}$ of our spectrometer (see Supplement B). Then, using a Helium gas tube, we measured diffraction angles with respect to the zeroth-order fringe, and used Eq. 2 to solve for λ of the spectrum. By comparing these observed angles to NIST standard vacuum wavelengths, we performed a least-squares fit to calculate a more precise value for d, using that for subsequent measurements of known gases: Mercury, Hydrogen, and Xenon, alongside using Argon gas to verify angular dispersion theory for a pixel-to-wavelength conversion.

3.3 Unknown Gas Identification

The final stage of the experiment involved the analysis of an unknown gas discharge tube [2]. We recorded the diffraction angles for the most prominent emission lines and converted these to wavelengths using the refined d value. We then compared our experimental spectrum to a library of known gas spectra to determine the identity of the unknown sample.

4 Data Analysis and Results

4.1 Grating Calibration: Laser and Helium

We characterized the spectrometer by using a crude measurement of the grating constant d using the monochromatic laser source, finding $d = 836.5 \pm 3.7$ nm, within 1σ of the manufacturer's value of 833.3 nm [2]. To refine this calibration, we measured the emission spectra of He I, and used NIST wavelength values to plot $m\lambda$ vs. $\sin(\alpha)$. Performing an ODR fit on this data yielded a value of 834.4 ± 1.3 nm, also within 1σ of the nominal value [2]. The calibration plots and the analysis of the errors associated with them are located in Supplement C.

4.2 Spectral Verification of Known Gases

First, we use Argon gas to verify the angular dispersion theory and to establish a pixel-to-wavelength conversion, detailed in Supplement D. Then, using the calibrated grating constant, we verified the visible emission lines for H I, Hg I, and Xe I. We verify the spectral lines using the spectral plots and reduced χ^2 calculations, as detailed in Supplement E. We find reduced χ^2 values of 3.0, 3.0, and 2.3, respectively, indicating good fits to the true spectrum, and verifying the accuracy of our spectrometer.

4.3 Analysis of Unknown Gas

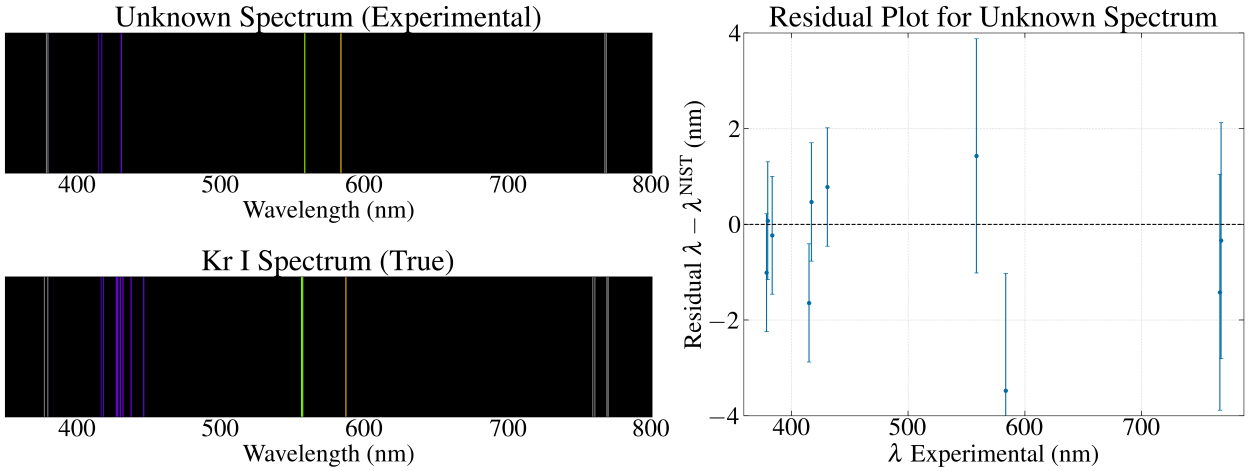

Figure 2: Our spectrum against the Krypton spectrum (left) and the residual plot comparing the two (right). We see good visual agreement with the spectrum and quantitative analysis returns a reduced $\chi^2 = 0.54$, indicating a good fit to the true spectrum. Our residual plot shows no discernible pattern, with a random scatter above and below the horizontal. The errors are detailed in Supplement F, and we see all points are within 2σ of the horizontal.

An unknown discharge tube, characterized by a lavender emission color, was analyzed. We used the NIST database to analyze four possible gases: Krypton, Nitrogen, Xenon, and Sodium. The quantitative analysis is detailed in Supplement F. From qualitative analysis, knowing our gas tube glowed a lavender color, we suspect Krypton is our gas. Using quantitative analysis, we find a reduced χ^2 of 0.54 for our spectrum compared to Krypton, indicating a good fit, and significantly closer to unity compared to the other contenders with $\chi^2 >> 1$. The spectrum is shown in Fig. 2 with a residual plot. The residual plot has errors detailed in Supplements E and F, and from the plot we can see a random spread of points above and below the horizontal with no discernible shape, with all points being within 1 or 2σ of no residual.

5 Discussion and Conclusions

In this experiment, we calibrated a visible spectrometer to perform precision atomic spectroscopy. By employing the Littrow configuration, we established a grating constant $d = 834.4 \pm 1.3$ nm, within 1σ of the manufacturer's value of 833.3 nm [2]. This calibration was validated against the known spectra of Xenon, Mercury, and Hydrogen. We retrieved reduced χ^2 for all three close to unity, indicating good fits to the true spectrum, and verifying the precision of our spectrometer.

We utilized Argon gas to verify angular dispersion theory and create a pixel-to-wavelength calculation. With this additional calibration, we were able to identify the unknown gas sample as Krypton, due to a good reduced $\chi^2 = 0.54$ and due to visual and qualitative agreement. The results confirm that even with a manual spectrometer, the application of precise mathematical models and digital processing can achieve wavelength calculation accuracy and identification of unknown elements.

These calibration techniques are fundamental to modern astrophysics. Because astrophysical objects are too distant to visit, light is our only source of information, and spectroscopy acts as the "DNA analysis" of the universe. For example, by comparing the emission and absorption lines observed in stellar spectra to the NIST database used in this lab, astronomers can determine the chemical composition of distant stars [4]. The strength and width of these lines reveal the temperature, pressure, and metallicity of a star, which in turn tells us its age and life-cycle stage [4].

References

[1] Haken H. and Wolf H. C. The Physics of Atoms and Quanta: introduction to Experiments and Theory (Springer, 7th ed.), (2005).

[2] READ ME: Visible Spectroscopy Experiment, Carmen/Canvas, (2024).

[3] Kramida, A., Ralchenko, Y., Reader, J., and NIST ASD Team. NIST Atomic Spectra Databse (ver. 5.11), (2023). https://physics.nist.gov/asd.

[4] Ryden, B. and Peterson, B. M. Foundations of Astrophysics, (Cambridge University Press, Cambridge, 2020).

[5] Thorlabs, Inc., Zelux 1.6 MP CMOS Compact Scientific Digital Cameras User Guide, (2020). https://www.manualslib.com/manual/2565019/Thorlabs-Cs165-Series.html?page=2#manual.

Supplement

A Grating Equation Derivation

Imagine a plane wave of monochromatic, collimated light with wavelength λ hitting a diffraction grating at an angle α. A diffraction grating consists of a large number of parallel grooves separated by a distance d, known as the grating spacing. When the light shines on the grating, it diffracts at another angle β. This is shown in Fig. A.1.

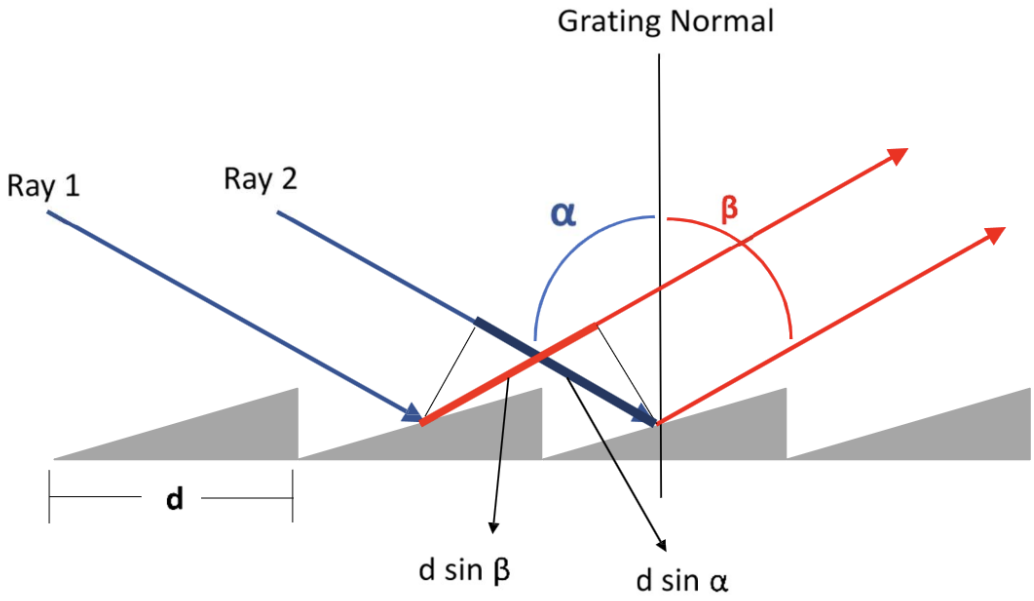

Figure A.1: Diagram of the grating [2]. We see incoming parallel rays at an incident angle α and their outgoing rays diffracted at a new angle β [2]. As shown in the diagram, the path length difference (PLD) for the incoming light is $d\sin(\alpha)$ and the PLD for the diffracted light is $d\sin(\beta)$ [2].

If we define all incident angles relative to the grating normal to be positive (meaning $\alpha > 0$), and the diffracted angles to be negative ($\beta < 0$), then we can analyze the path length difference (PLD), or the difference the light travels on the way in and the way out [2]. Using the trigonometry shown in Fig. A.1, we can define the PLD as [2]

$$\text{PLD} \equiv \Delta l = d\sin(\alpha) + d\sin(\beta). \tag{A.1}$$

As is typical for problems with interference and diffraction, we concern ourselves with locations of constructive and destructive interference [2]. By this principle, total constructive interference will occur at the angles where the PLD between rays is equal to an integer multiple of the wavelength

λ [2]. If we call this integer m, then we can see that [2]

$$\text{PLD} = m\lambda. \tag{A.2}$$

Equating these two yields the grating equation,

$$\boxed{d(\sin(\alpha) + \sin(\beta)) = m\lambda.}$$

This is the grating equation, showing that for a given incident wavelength and angle, we can have multiple bright fringes based on the integer m at differing angles β [2]. The m value corresponds to a different order of fringe, with the first order being $m = \pm 1$, and so forth [2]. For this experiment, we consider the Littrow configuration, where $\alpha = \beta$, and hence [2]

$$2d\sin(\alpha) = m\lambda. \tag{A.3}$$

B Spectrometer Resolution

In Fig. B.1, we see the resolution of the two spectral lines of Na I at 589.0 and 589.6 nm [3]. We utilize the equation for the resolving power $\mathscr{R}$ of a spectrometer [2]

$$\mathscr{R} = \frac{\lambda}{\Delta\lambda}, \tag{B.1}$$

where λ is the average wavelength of the spectral lines and $\Delta\lambda$ is the limit of the resolution.

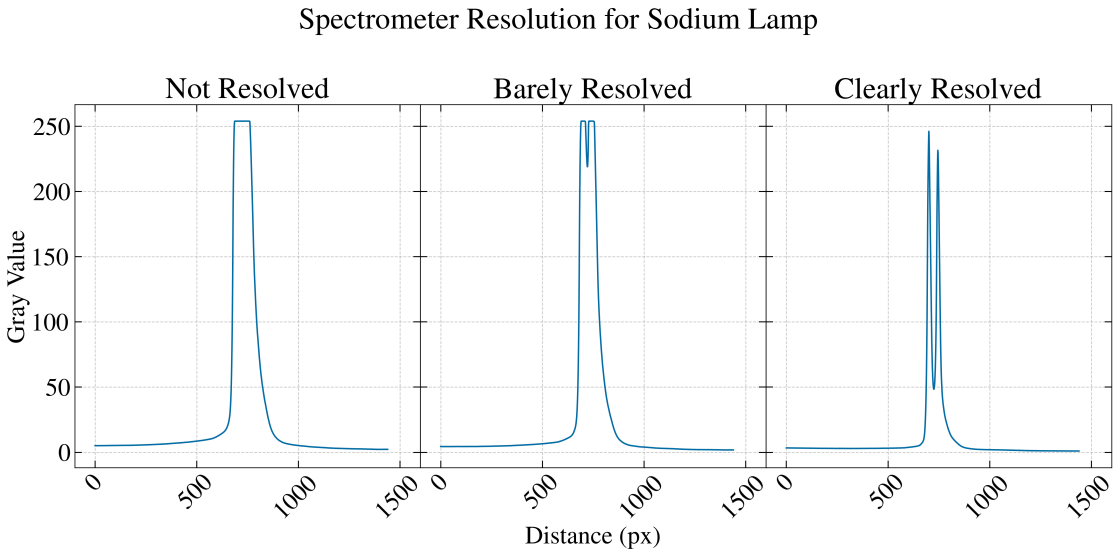

Figure B.1: Resolution of the two Na I spectral lines at 589.0 and 589.6 nm, for cases of not being resolved, barely resolved, and clearly resolved [2, 3]. We calculate resolving powers of ~ 397, ~ 460, ~ 2161, respectively. We note that the "Not Resolved" and "Barely Resolved" cases display significant saturation. This saturation of CCD pixels at wider slit settings led to an overestimation of the spectral width and underestimation of resolving power.

In our "Clearly Resolved" data, the peaks are separated by 44 pixels, which allows us to set a resolution scale related to the separation of the two lines $\Delta\lambda_{\text{sep}} = 0.6nm$. This can give us a resolution scale $S = 0.6$ nm$/44$ px $= 0.014$ nm$/$px. Then, we can calculate $\Delta\lambda$ for Eq. B.1 using the full-width half-maximum (FWHM) of a single peak, and use the resolution scale such that

$$\Delta\lambda = \text{FWHM}_{\text{pixels}} \times S. \tag{B.2}$$

Using numerical analysis, we can find the peaks and their FWHM, and thus the resolving power $\mathscr{R}$, tabulated in Table B.1.

Case	FWHM (px)	FWHM (nm)	$\mathscr{R}$
Not Resolved	109.0	1.486	396.5
Barely Resolved	94.0	1.282	459.7
Clearly Resolved	20.0	0.273	2160.8

Table B.1: Tabulated resolving power $\mathscr{R}$ values using numerical FWHM calculations and the calculated resolution scale S.

An important note is that the "Not Resolved" and "Barely Resolved" cases show significant saturation. The saturation of CCD pixels at wider slit settings led to an overestimation of the spectral width. For future measurements, we ensure to resolve lines properly to avoid this effect [2].

C Grating Spacing & Its Error Analysis

To calculate the grating spacing d for the laser, we set the grating dial to $0°0'$ at the zeroth-order fringe. We then rotate and record the $m = \pm 1$ fringes. We then use the Littrow configuration equation to solve for d. We get that both fringes occur at $18°$, and as such we get a d values of 836.5 nm. We can then propagate the error for this by using the equation for d from the Littrow configuration of

$$d = \frac{\lambda}{2\sin(\alpha)}, \tag{C.1}$$

since we are using $|m| = 1$.

Since $\lambda = \lambda_{\text{laser}} = 517$ nm is constant, we can get the error on d, σ_d, through error propagation:

$$\sigma_d = \left|\frac{\partial d}{\partial \alpha}\right| \sigma_\alpha = \frac{\lambda\cos(\alpha)}{2\sin^2(\alpha)}\sigma_\alpha. \tag{C.2}$$

We use a constant σ_α of $5'$ from the angular resolution of our diffraction grating. Doing as such yields our error of 3.7 nm, yielding a laser d value of 836.5 ± 3.7 nm, within 1σ of the manufacturer's 1200 grooves/mm, which equates to $d = 833.3$ nm [2].

For the Helium calibration, we calculate the constituent wavelengths of the He I spectrum. We then plot those on a graph and use an Orthogonal Distance Regression (ODR) fit to extract the d value. That plot is shown in Fig. C.1, yielding $d = 834.4 \pm 1.3$ nm, also within 1σ of the expected value, with a lower percent error and higher accuracy [2]. For the ODR fit, we use the propagation of errors formula. For the x-axis, we use a constant σ_α of $5'$ from the resolution of our diffraction grating. Then,

$$\sigma_{\sin(\alpha)} = \left|\frac{\partial \sin(\alpha)}{\partial \alpha}\right| \sigma_\alpha = \cos(\alpha)\sigma_\alpha. \tag{C.3}$$

The y-errors use a similar setup. Since our experimental wavelength values were calculated from our laser d value, we use $\sigma_d = 3.7$ nm alongside the same σ_α. Then,

$$\sigma_{m\lambda} = \sqrt{\left(\left|\frac{\partial(m\lambda)}{\partial\alpha}\right|\sigma_\alpha\right)^2 + \left(\left|\frac{\partial(m\lambda)}{\partial d}\right|\sigma_d\right)^2} = \sqrt{4d^2\cos^2(\alpha)\sigma_\alpha^2 + 4\sin^2(\alpha)\sigma_d^2}. \tag{C.4}$$

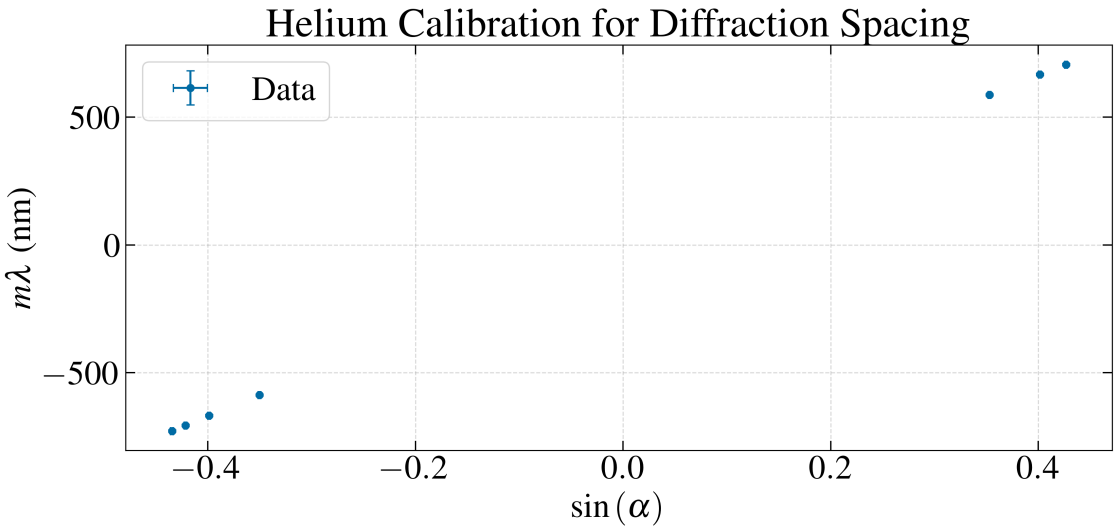

Figure C.1: Plot of $m\lambda$ of experimental wavelength calculations of the He I spectrum vs. the experimental $\sin(\alpha)$ values. We fit an ODR fit to this data, with x- and y-errors calculated via Eqs. C.3 and C.4. The errors are too small to be seen on the plot. This fit yielded $d = 834.4 \pm 1.3$ nm, within 1σ of the nominal value of 833.3 nm, and with a lower percent error compared to the laser calibration value [2]. The fit returned a reduced χ^2 of 0.3, indicating a good fit to the data.

D Argon Pixel to Wavelength Conversion

We calculate a pixel-to-wavelength conversion factor using an Argon gas tube. We use two snapshots of Argon gas at $\alpha = 29°0'$ and $\alpha = 333°5'$, as in Fig. D.1. These α values would be for the center of the image with the multiple spectral lines.

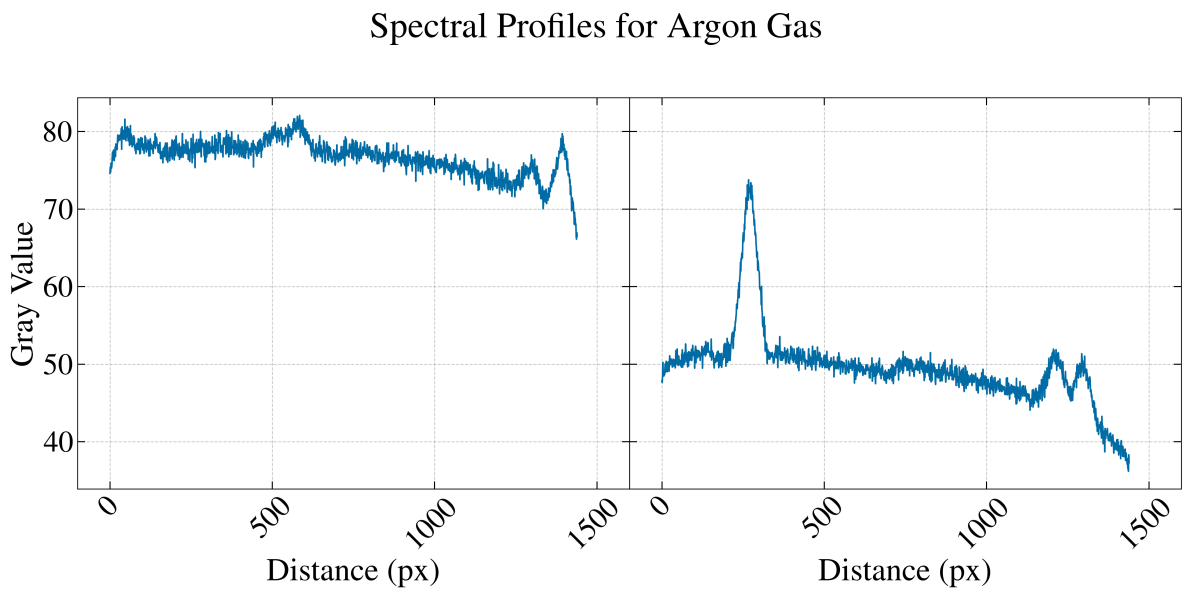

Figure D.1: Two profile plots of Argon gas. The left plot is at $\alpha = 29°0'$ for $m = 1$ and the right plot is $\alpha = 333°5'$ for $m = -1$. We fit the 5 visible peaks on the left plot and the three visible peaks on the right plot to a Gaussian distribution to locate the centroid [2]. Once the centroid is located, we can calculate the pixel-to-wavelength conversion by using the NIST database to find the λ values of the spectral lines shown [2].

Based on the Littrow configuration, we can calculate the wavelength of the central position of the grating, calculating $\lambda \approx 809$ nm and $\lambda \approx 755$ nm, respectively, using $d = 834.4$ nm. Our camera can detect lines in the IR [5]. Calculating the centroid positions of a Gaussian, via

$$f(x, A, \mu, \sigma) = Ae^{-\frac{(x-\mu)^2}{2\sigma^2}}. \tag{D.1}$$

Using SciPy's curve fit algorithm, we can use the data from Fig. D.1 to find the locations of the centroids. Then using the NIST dataset, we can find the wavelengths of each peak. This is tabulated in Table D.1.

α	Centroid (px)	λ (nm) [3]
$29°0'$	55.42	794.8176
$29°0'$	509.10	800.6157
$29°0'$	577.73	801.4786
$29°0'$	1292.06	810.3693
$29°0'$	1388.75	811.5311
$333°5'$	270.43	738.3980
$333°5'$	1212.11	750.3869
$333°5'$	1290.67	751.4652

Table D.1: Tabulated values for centroid values in pixels from Fig. D.1, with λ values for Argon gas from NIST [3]. We use these values to calculate the linear dispersion $\frac{dx}{d\lambda}$ in px/nm.

We fit Table D.1 to a linear model. In doing so, we can extract the slope to get the pixel-to-wavelength conversion. This fit yielded a pixel-to-wavelength conversion of 79.89 px/nm for $\alpha = 29°0'$ and 78.27 px/nm for $\alpha = 333°5'$. These fits yielded a linearity R^2 of 0.99994 and 0.99997, respectively, indicating a strong linear relationship.

Theoretically, in the Littrow configuration, the angular dispersion is given by [2]:

$$\frac{d\alpha}{d\lambda} = \frac{m}{2d\cos(\alpha)}. \tag{D.2}$$

Hence, the linear dispersion of our detector (in px/nm) is calculated by multiplying this by the camera's angular resolution $\frac{dx}{d\alpha}$, or

$$\frac{dx}{d\lambda} = \left(\frac{dx}{d\alpha}\right) \cdot \frac{m}{2d\cos(\alpha)}. \tag{D.3}$$

We found our angular range of $40'$ by tracking spectral lines from the left side to the right side of the camera view, and calculating the angular displacement of the grating. Hence, based on this theory, we would anticipate that the second order dispersion would be double that of the first order, since $\frac{dx}{d\lambda} \propto m$. We also note that the conversion factor is higher at $29°0'$ than at $333°5' = -26.92°$. This matches the theory, where the dispersion increases as $1/\cos(\alpha)$. In fact, our ratio of experimental slopes ($79.89/78.42 = 1.021$) is in excellent agreement with the theoretical ratio ($\cos(26.92°)/\cos(29°) = 1.019$, confirming the validity of our calibration. For this report, we will use a pixel-to-wavelength conversion of 79.1 px/nm for $|m| = 1$.

E Known Gas Spectra

Below are the spectral distributions we retrieved from our experimental data and the ones from the NIST database. We use the Helium-calibrated d value of 834.4 nm for these calculations. For these spectra, we can quantitatively measure how good our fit is by calculating the reduced χ^2:

$$\chi^2 = \sum_{i=1}^{N} \frac{(\lambda_i - \lambda_i^{\text{NIST}})^2}{\sigma_i^2}, \tag{E.1}$$

where σ_i is the error in the measurement. We calculate σ_i through the propagation of errors in λ:

$$\sigma_\lambda = \sqrt{\left(\left|\frac{\partial\lambda}{\partial\alpha}\right|\sigma_\alpha\right)^2 + \left(\left|\frac{\partial\lambda)}{\partial d}\right|\sigma_d\right)^2}. \tag{E.2}$$

We utilize σ_d from our Helium d calculation for $\sigma_d = 1.3$ nm. For σ_α, we use the discretization of our diffraction grating of $5'$. This gives us the formula,

$$\sigma_\lambda = \sqrt{\frac{4\sin^2(\alpha)}{m^2}\sigma_d^2 + \frac{4d^2}{m^2}\cos^2(\alpha)\sigma_\alpha^2}. \tag{E.3}$$

With this equation, we can now calculate the reduced χ^2 for each spectrum.

We analyzed the spectra of Mercury, Hydrogen, and Xenon, in Figs. E.1 - E.3. We only included the spectral lines relevant to our experimental result, not the entire spectrum. We calculate χ^2 values of 3.0, 3.0, and 2.3, respectively, indicating good fits to our data.

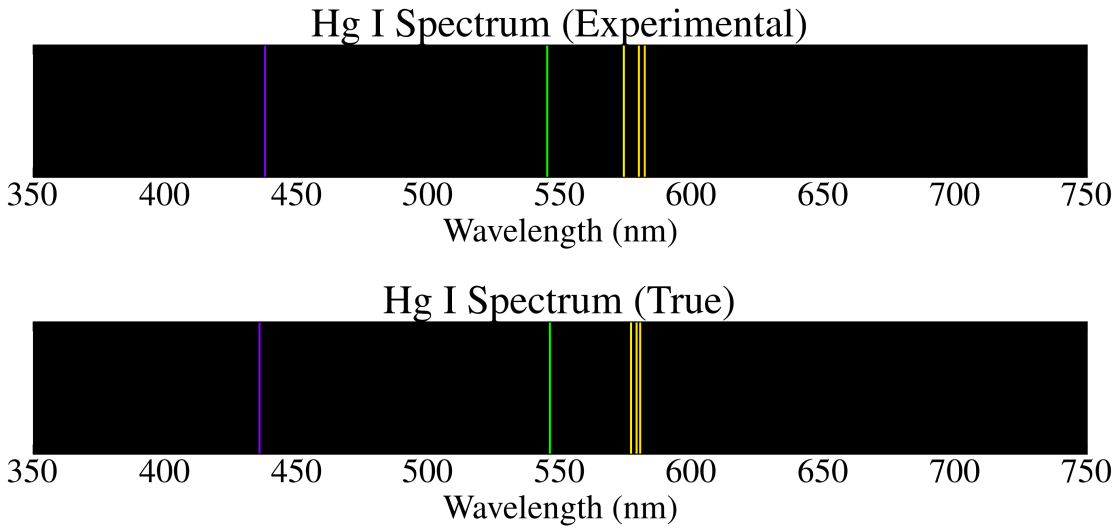

Figure E.1: Spectrum of Hg I (top=experimental, bottom=true from NIST) [2, 3]. We see good visual agreement with the two spectral distributions. The reduced χ^2 for our spectrum is 3.0, indicating a good fit to the data.

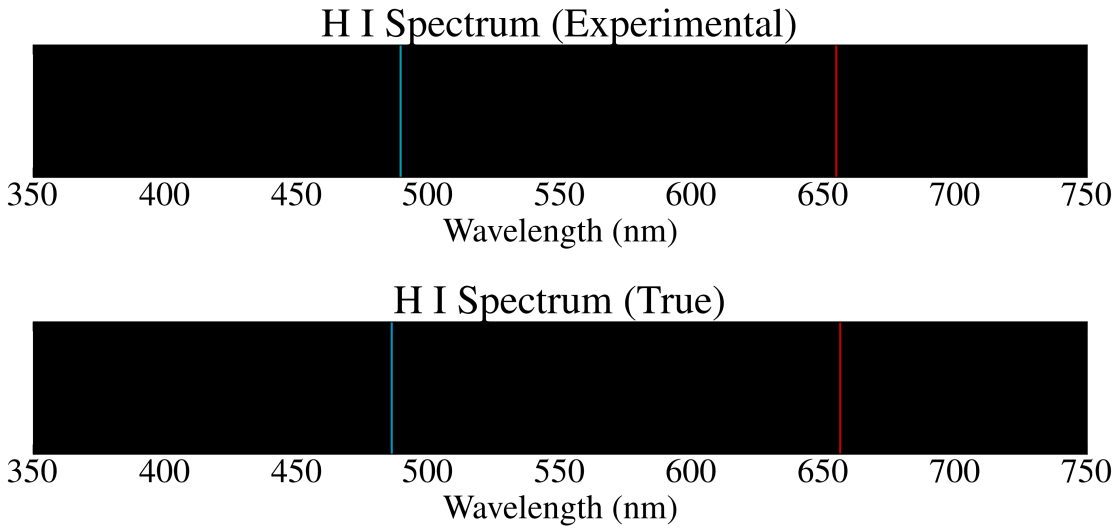

Figure E.2: Spectrum of H I (top=experimental, bottom=true from NIST) [2, 3]. We see good visual agreement with the two spectral distributions. Our reduced χ^2 is 3.0, indicating a good fit to the data, which is slightly accentuated by the fact that we only have two lines to work with.

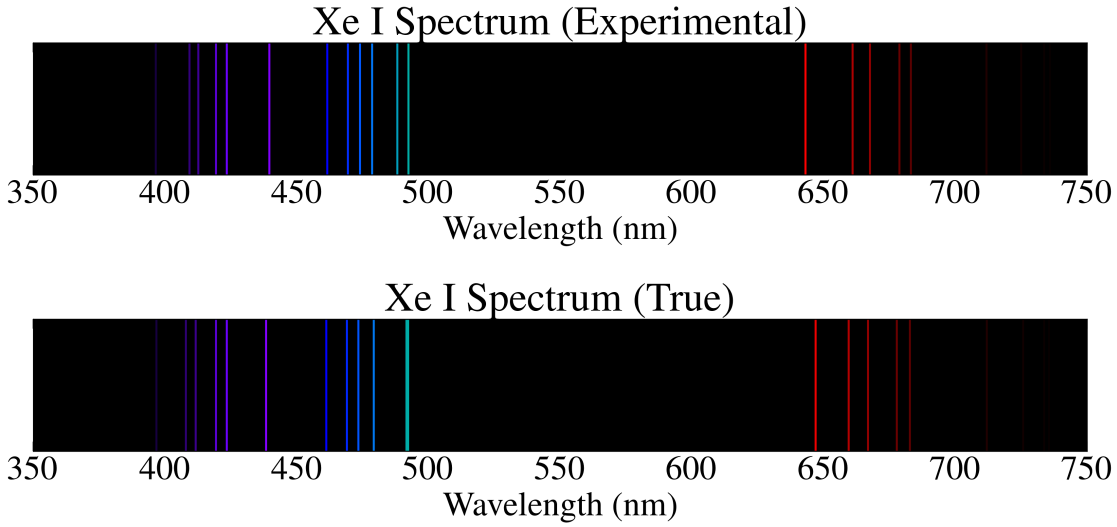

Figure E.3: Spectrum of Xe I (top=experimental, bottom=true from NIST) [2, 3]. We see good visual agreement with the two spectral distributions. Our reduced χ^2 was 2.3, indicating a good fit to the data, especially given the number of lines present and recorded.

We can also make residual plots. For each of the residual plots, the errors are σ_λ from above. For all plots, in general, we see that residuals are randomly scattered above and below 0 with no discernible pattern or shape. We can also see that most data points lie within 1 or 2σ. We can see how deviations in the Hg and H spectra cause increased χ^2 values from a lack of total data points.

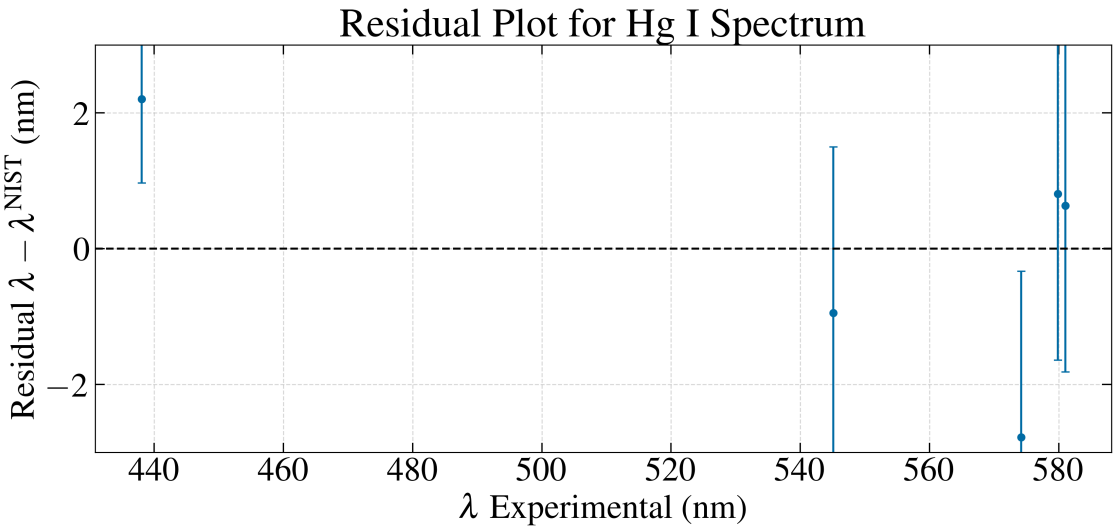

Figure E.4: Our residual plot for the Hg I spectrum, with error bars from Eq. E.3. We see a good spread of residuals above and below the horizontal, with no discernible shape, and all error bars within 1 or 2σ of no residual.

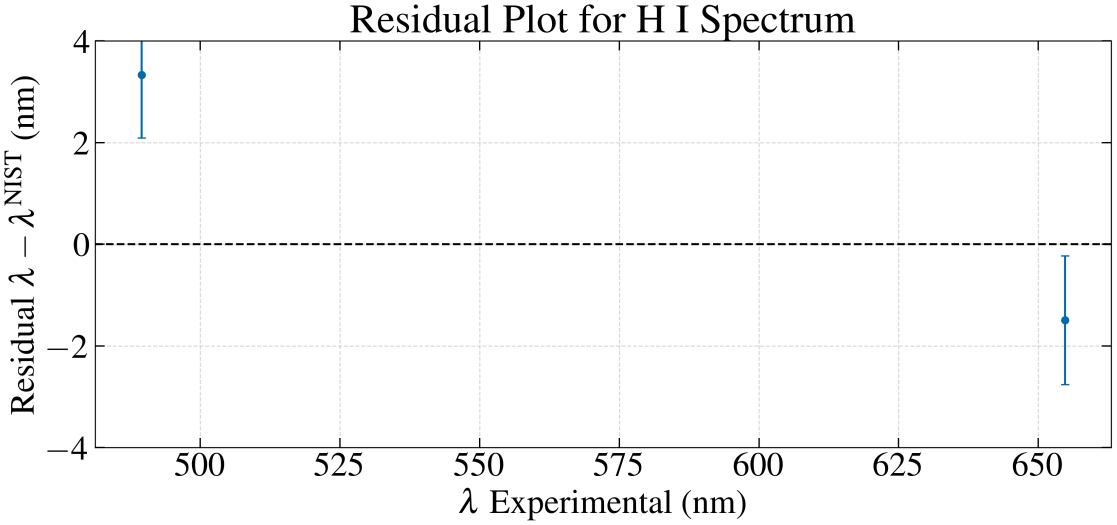

Figure E.5: Our residual plot for the H I spectrum, with error bars from Eq. E.3. We see a good spread of residuals above and below the horizontal, with no discernible shape, and all error bars within 2σ of no residual. Having only two data points with 2σ residuals shows why the reduced χ^2 is accentuated for this spectrum.

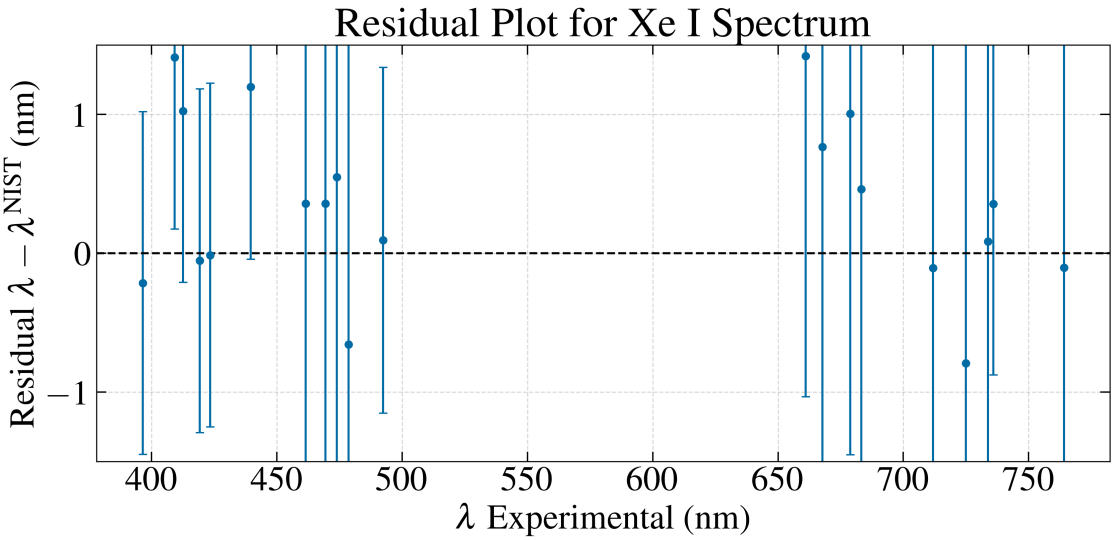

Figure E.6: Our residual plot for the Xe I spectrum, with error bars from Eq. E.3. We see a good spread of residuals above and below the horizontal, with no discernible shape, and all error bars within 1 or 2σ of no residual. We see a lot of data points close to the horizontal, displaying the goodness of our χ^2 result.

F Unknown Gas Identification Addendum

We consider the following gases, using the NIST database: Krypton, Nitrogen, Xenon, and Sodium. The best three spectra (meaning excluding NItrogen) are shown in Fig. F.1. From visual inspection, it does seem that Krypton most closely resembles our gas of choice.

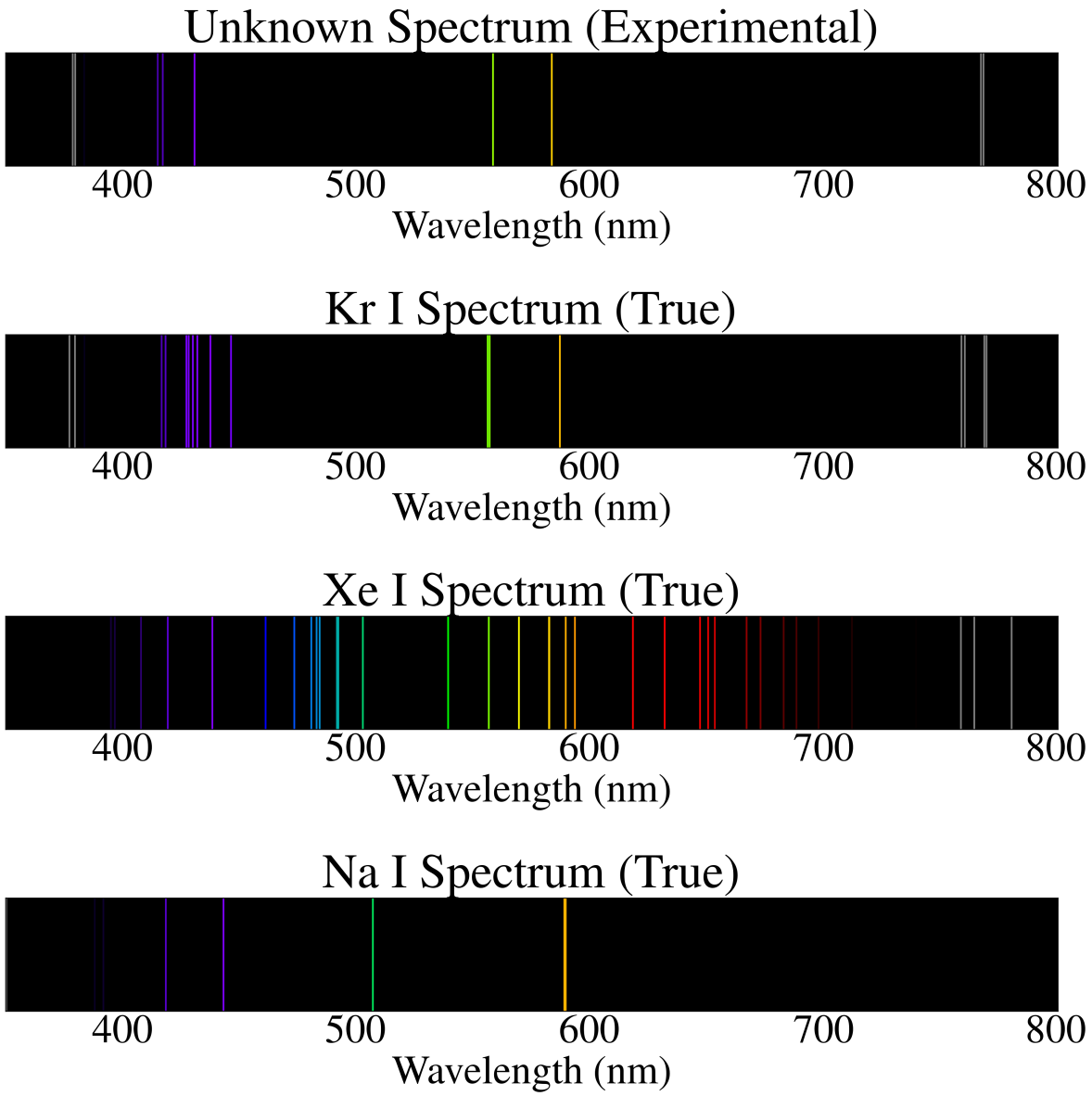

Figure F.1: Spectral distributions from our experimental spectrum (top), and the three best fits (Krypton, Xenon, and Sodium) [3]. Nitrogen was left out due to a considerably higher reduced χ^2 value than the rest. Visually, we see that the Kr spectrum most closely resembles our experimental result. Calculating the reduced χ^2 for these spectra yields 0.54 (Kr), 18.10 (Xe), and 47.04 (Na). From this, we can determine quantitatively that our unknown gas is most likely Krypton. We can also note qualitatively that our gas glowed a lavender color, typical of a Krypton gas.

Mathematically, we use the reduced χ^2 to quantitatively decide which spectrum fits the best (see Supplement E for the formulation). Calculating the reduced χ^2 from the formulae in Supplement E, we get the results in Table F.1.

Gas	Reduced χ^2
Krypton (Kr)	0.54
Nitrogen (N)	120.39
Sodium (Na)	47.04
Xenon (Xe)	18.10

Table F.1: Tabulated reduced χ^2 from NIST spectra of Krypton, Nitrogen, Sodium, and Xenon, compared to our experimental spectrum. We see that the best fit χ^2 is the Krypton spectrum, indicating statistically that our gas is likely Krypton gas.

From the reduced χ^2, we can see that the Nitrogen, Sodium, and Xenon values have $\chi^2 >> 1$, indicating that our experimental spectral lines do not match those spectra very well. The Krypton spectrum χ^2 of 0.54 indicates a good fit to the data, providing statistical evidence of Krypton being our gas.

On a qualitative note, we noted that the gas was indeed a gas at room temperature and was glowing a lavender color. We note that a Sodium gas tube, a Nitrogen gas tube, and a Xenon gas tube don't glow quite this color, but a Krypton gas tube does, providing a qualitative justification for Krypton being our gas.